Journal of the Korean Society for Nondestructive Testing
Vol. 30, No. 3 (2010. 6)

Imaging of a Defect in Thin Plates Using the Time Reversal of Single Mode Lamb Wave: Simulation

Hyunjo Jeong*†, Jung-Sik Lee*, Sung-Min Bae* and Hyun-Ki Lee*

Abstract This paper presents an analytical investigation for a baseline-free imaging of a defect in plate-like structures using the time-reversal of Lamb waves. We first consider the flexural wave (A0 mode) propagation in a plate containing a defect, and reception and time reversal process of the output signal at the receiver. The received output signal is then composed of two parts: a directly propagated wave and a scattered wave from the defect. The time reversal of these waves recovers the original input signal, and produces two additional side bands that contain the time-of-flight information on the defect location. One of the side band signals is then extracted as a pure defect signal. A defect localization image is then constructed from a beamforming technique based on the time-frequency analysis of the side band signal for each transducer pair in a network of sensors. The simulation results show that the proposed scheme enables the accurate, baseline-free detection of a defect, so that experimental studies are needed to verify the proposed method and to be applied to real structure.

Keywords: Defect Detection(Imaging), Lamb(Flexural) Wave, Time Reversal, Flaw Scattering, Time-Frequency Analysis, Base-Line Free Detection, Sensor Network, Beamforming

1. Introduction

Defect (or damage) location and characterization are becoming increasingly important in the area of structural health monitoring(SHM) of aerospace and civil structures. The structural members in those applications are platelike shapes, so that nondestructive evaluation(NDE) of guided waves such as Lamb waves have gained extensive attention (Giurgiutiu, 2008). Guided waves can propagate long distances with little amplitude loss. Various methods for Lamb wave damage detection include pulse-echo method (Rose et al., 1994; Alleyne et al., 2001; Giurgiutiu et al., 2004), pitch-catch method (Prasad, 2004; Tua et al., 2005; Park et al., 2006; Cuc et al., 2009; Ihn and Chang, 2008), and more recent time reversal(TR) method (Ing and Fink, 1998; Wang et al., 2004; Sohn et al., 2007; Santani et al., 2007).

Due to the multimodal and dispersive nature of Lamb waves, it is sometimes difficult to analyze measured responses. Signal processing and dispersion curves have been used to understand the complex Lamb waves and help defect detection. The time reversal method is a new approach developed to mitigate Lamb wave dispersion and increase the applicability of Lamb waves for SHM. The effect of dispersion on the time reversal analysis of Lamb waves was first studied by Wang et al. (2004) by introducing the time reversal operator into the Lamb wave equation based on the Mindlin plate theory. Recent work by Park et al. (2009) further

Received: April 5, 2010, Revised: May 17, 2010; June 7, 2010, Accepted: June 10, 2010. *Division of Mechanical and Automotive Engineering, Wonkwang University, Iksan, Jeonbuk 570-749, Korea, †Corresponding Author: hjjeong@wonkwang.ac.kr

enhanced the time reversal method by using a tone burst signal in a single and multiple modes TR process.

Initial applications for the time reversal method in flaw or damage detection were aimed at increasing Lamb wave resolution by using time reversal mirrors (Ing and Fink, 1998). Unlike most other SHM techniques, the time reversal process introduces a baseline-free method for damage detection. When nonlinear damages are present, the linear reciprocity of the system breaks down and the difference between the original input signal and the reconstructed TR signal can be an indicator for the presence of damage. Improvement to the damage detection algorithm was made by first incorporating extreme value analysis (Sohn et al., 2004), and later enhanced by adding consecutive outlier analysis to decrease the possibility of false damage alerts.

In this paper, we present an analytical investigation for defect localization imaging (detection and location) in plate-like structures using the time reversal analysis of flexural waves. The flexural wave used is the A_0 mode Lamb wave and its transfer function for a circular piezoelectric source is based on the Mindlin plate theory. We consider the scattering of flexural waves from linear defects such as through holes in propagation and time reversal process of output signals for each transducer pair. The proposed method employs the time reversal of flexural waves and a beamforming technique using a distributed network of transducers operating in a pitch-catch mode. The time reversal of the output signal which contains the direct and scattered waves exactly recovers the original input signal and produces additional side bands. One of the side band is used to construct the baseline-free defect localization image. Based on the fundamental idea of the beamforming method with a distributed sensors, the signal-to-noise ratio of the defect image is greatly improved, and very accurate defect location can be obtained.

2. Propagation of a Single Mode Lamb Wave and TR Process

Fig. 1 shows the components of an ultrasonic testing situation for damage/defect detection and localization where a flaw is being interrogated in a pitch-catch arrangement using a network of piezoelectric(PZT) transducers. In order to simulate the potential of a time reversal method as an effective means of identifying damage in large plate-like structures, four identical PZT patches of a circular shape are employed and mounted on the corners of 300 mm × 300 mm square area. They are used interchangeably as actuators or sensors. We assume an omni-directional radiation pattern of the circular PZT actuator in both near and far fields.

When the flexural Lamb wave is generated at sensor A and travels along the plate containing a defect, the forward propagating wave will arrive at sensor B through two different paths, as shown in Fig. 2. In Fig. 2, P1 and P2 represent direct and scattering paths. The response voltage obtained at sensor B through the direct path P1 can be written in the frequency domain as

$$V_{B1}(\omega) = G_1 K_a K_s V_A \tag{1}$$

where V_A is the input at patch A, K_a and K_s, the mechanical-electro efficiency factor of sensor A and B, and G_1 the frequency response function of sensor B as a result of the input at

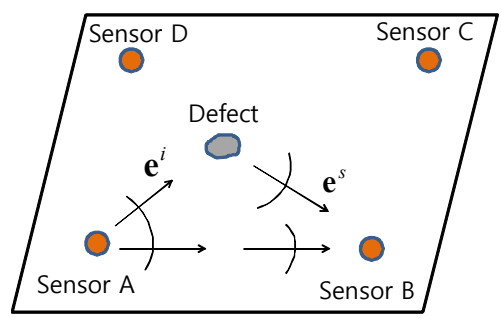

Fig. 1 Lamb wave based defect localization using a network of sensors

sensor A. The frequency response function G_1 for the A_0 mode Lamb wave is obtained by applying appropriate transformation techniques in the spatial and time domain to the wave equation based on the Mindlin plate theory (Wang et al., 2004)

$$G(r,\omega) = -\frac{i\pi h^2}{2D}\frac{r_1 k_1^s a J_2(k_1 a) H_0^{(1)}(k_1 r)}{k_1^2 - k_2^2} \quad (2)$$

where r is the wave propagation distance and ω is the circular frequency. In eqn. (2), h, D, γ_1, a, $J_1(\cdot)$ and $H_0^1(\cdot)$ are the plate thickness, the flexural stiffness of the plate, the amplitude ratio of dilatational to shear wave potentials at the wave number k_1, radius of sensor A, the first order Bessel function and the zeroth order Hankel function of the first kind, respectively. The wave numbers k_1 and k_2 are determined at the A_0 and A_1 modes of the Lamb waves, respectively.

On the other hand the response signal at sensor B through the scattering path P2 can be described by

$$V_{B2}(\omega) = G_{1s} G_{s2} A K_a K_s K_s V_A = G_2 K_a K_s V_A \quad (3)$$

where $G_2 = G_{1s} G_{s2} A$. Here, G_{1s} and G_{s2} are the transfer functions for wave propagation paths from actuator 1 to the scatterer and from the scatterer to sensor 2, respectively, and A is the far field scattering amplitude which completely describes the scattered wave field. The scattering amplitude generally depends on the incident wave direction $\mathbf{e}^i$ as well as the scattering direction $\mathbf{e}^s$. A also depends on the frequency ω. The flaw embedded in the plate can be of arbitrary shape or material, however, we assume scatterers of circular shape, so that the reciprocity of scattering holds.

The time reversibility of wave is based on the spatial reciprocity and time reversal invariance of linear wave equations. In the time reversal method, an input signal can be reconstructed at an excitation point (point A) if an output signal recorded at another point (point B) is reemitted to the original source point (point A) after being reversed in the time domain as illustrated in Fig. 2.

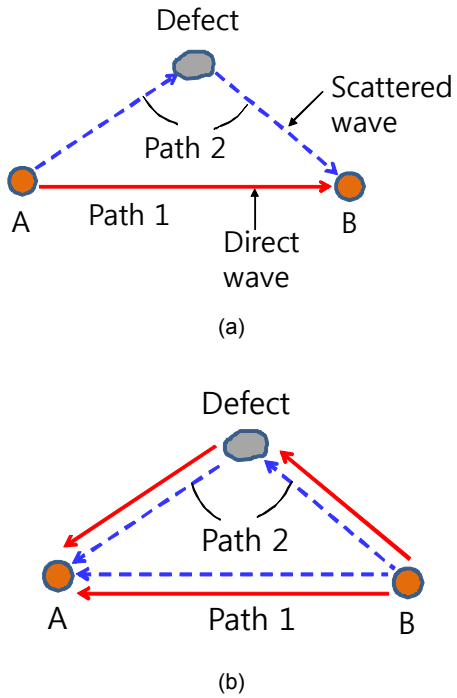

Fig. 2 Flexural wave propagation in a plate containing a defect: (a) Forward propagation from sensor A includes direct and scattered waves, and (b) Backward propagation from sensor B after reception and time reversal

Once a response signal is measured at sensor B, the reconstructed input signal at sensor A can be obtained by reemitting the time-reversed response signal at sensor B. The time reversal operation of a signal in the time domain is equivalent to taking the complex conjugate of the Fourier transform of the signal in the frequency domain. There are four possible propagation paths when the received signal at sensor B is time reversed and reemitted to reach sensor A. Therefore, the reconstructed signal at sensor A from the reemitted signal at sensor B can be written as (Jeong, 2010)

$$\begin{aligned} &\nu_R(t) \\ &= \sum_{m=1}^{2} \overline{C}_{mn}\overline{K}V_A(T-t) \\ &+ \sum_{m=1}^{2}\sum_{n=1}^{2}(1-\delta_{mn})\overline{C}_{mn}\overline{K}e^{i\overline{\omega}\overline{\tau}_{mn}}V_A[T-(t-\overline{t_{mn}})] \end{aligned} \tag{4}$$

where $\overline{C}_{mn}$ are related to the amplitudes of forward and time reversed backward propagating waves for different paths and $\overline{K}$ denotes the mechanical-electro efficiency factors for actuator and sensor. In eqn. (4), $\overline{t_{mn}} = (r_m - r_n)/\overline{\nu_g}$ where r_m and r_n denote the propagation paths and $\overline{\nu_g}$ is the group velocity at the center frequency $\overline{\omega}$.

Eqn. (4) shows that the reconstructed signal is composed of four terms. The first two terms on the right hand side are produced when the time reversed direct and scattered waves travel back to sensor A (the original source position) along their respective forward propagation paths. They merge constructively at the same time to form a main part of the reconstructed voltage and thus represent the scaled and time-reversed version of the original input signal. It is noted that the reconstructed main signal have arrival time difference of $\bar{t}_{nm}$ compared to the second group of the reconstructed signal.

In addition to the reconstructed main signal, two other terms appear in eqn. (4). They represent the reconstructed signals when the direct and scattered waves travel along two different paths in the forward and backward propagation directions (i.e., P1->P2, P2->P1). The third term indicates the reconstructed voltage when the time reversed direct wave takes the path P2 in its back propagation to sensor A. Compared to the arrival time of the main signal, this wave will arrive later in time. The fourth term indicates the reconstructed voltage when the time reversed scattered wave takes the path P1 in its back propagation to sensor A. This wave will appear before the main signal. In other words, they are time shifted by $\bar{t}_{nm}$ and since $\bar{t}_{mn} = -\bar{t}_{nm}$ they create side bands with respect to the reconstructed main signal. The amplitude of side bands is proportional to $e^{i\overline{\omega}\overline{\tau}_{mn}}$, which can be interpreted as the phase shift. Furthermore, since $\bar{\tau}_{mn} = -\bar{\tau}_{nm}$ and $\bar{t}_{mn} = -\bar{t}_{nm}$ in eqn. (4), the reconstructed side bands are symmetric respect to the main signal.

The time shift $\bar{t}_{mn}$ between the main signal and the side band is actually the time-of-flight difference of propagating flexural wave between two paths (P1 and P2), so that this information will be utilized for defect localization (i. e., defect location and imaging).

3. Far-Field Scattering Amplitude of Flexural Waves

Consider scattering of a time-harmonic flexural wave by a small object located in a homogeneous isotropic plate. The scatterer may consist of a region with different plate properties (thickness, density, etc.) or it could be an attachment of some type. The scattered displacement of flexural wave at distance r can be expressed as:

$$W^{SC} = \frac{1}{\sqrt{2r}}e^{i(kr-\frac{\pi}{4})}A(e^i;e^s) + o(\frac{1}{\sqrt{r}}), \quad r\to\infty \tag{5}$$

where the scattering coefficient (or the far field scattering amplitude) $A(e^i;e^s)$ is defined such that

$$A(e^i;e^s) = \frac{2}{\sqrt{\pi k}}\Sigma_{n=0}^{\infty}(-1)^n A_n \cos n\theta \tag{6}$$

The flaw embedded in the plate can be of arbitrary shape or material, but it is assumed to be volumetric (noncracklike) in nature. In this case, the flaw scatters like a point source with an angular dependence coefficient $A(e^i;e^s)$, where e^i and e^s denote the incident wave direction and the scattering direction,

respectively. In this study, we assume scatterers of circular shape, so that the reciprocity of scattering holds.

The scattering coefficients in eqn. (6) can be found by applying appropriate boundary conditions at the interface between host plate and circular inclusion. For the case of limits where the heterogeneity is either rigid or soft (i.e. rigid inclusion or hole), these coefficients are obtained in closed forms (Norris and Vemula, 1995).

4. Baseline-Free TR Imaging of a Defect

A beamforming method can be used to construct a defect localization image (location and imaging) by relating the contrast at a particular pixel to the amplitude of the scattered signal received by all the sensors in the network. Consider a distributed network consisting of N active sensors, their positions being denoted by (x_i, y_i), i=1, 2, . . . N. The contrast S at a particular location or imaging pixel (x, y) can be expressed as

$$S(x,y) = \sum_{A=1}^{N}\sum_{B=1,B\neq A}^{N} W_{AB} f_{AB}(t_{AB}(x,y)) \tag{7}$$

where W_{AB} refers to the appropriate aperture weighting to each sensor pair and $f_{AB}(t)$ denotes the received scattered signal by sensor B due to the excitation of sensor A. Referring to Fig. 3, the arrival time t_{AB} of the scattered wave corresponds to the wave travel time from the actuator to the defect and then from the defect to the sensor is

$$t_{AB}(x,y) = \frac{[d_A(x,y) + d_B(x,y)] - d_{AB}}{\nu_g} \tag{8}$$

where

$$d_A(x,y) = \sqrt{(x_A - x)^2 + (y_A - y)^2}$$
$$d_B(x,y) = \sqrt{(x_B - x)^2 + (y_B - y)^2}$$

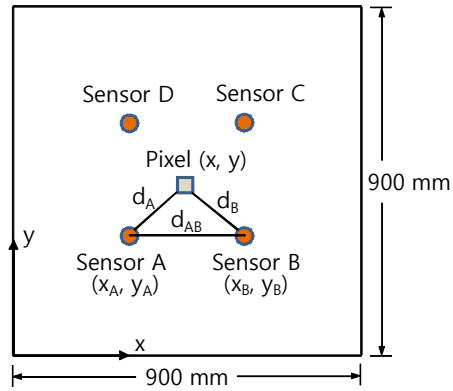

Fig. 3 A beamforming method to construct a defect localization image based on a distributed network consisting of four active sensors (d_{AB}=300 mm, coordinates of sensor A=(300 mm, 300 mm), B=(600 mm, 300 mm), C=(600 mm, 600 mm), D=(300 mm, 600 mm))

where d_A and d_B are the distance from the transducer A (actuator) to the defect and from the defect to the transducer B (sensor), respectively. d_{AB} is the direct distance from A to B. ν_g is the group velocity of the flexural Lamb wave. In the present case, three through-transmission signals can be obtained when one particular transducer is excited. Therefore there are a total of twelve different signals, corresponding to the twelve possible sensor pair combinations. The weighting factor of 1 will be used in this study by assuming uniform aperture weighting. To account for nonuniform aperture weighting, WAB is usually normalized by the maximum value of f_{AB}, i.e., $W_{AB} = \frac{1}{\max|f_{AB}|}$.

5. Simulation Results and Discussion

To simulate the plate theory solutions introduced in the proceeding section, a numerical example of flexural wave propagation and defect location is provided here. In particular, a narrow band excitation is employed, and the following input function is used.

$$y(t) = \begin{cases} [1-\cos(2\pi ft/N)]\cos(2\pi ft) & (0<t<N/f) \\ 0 & otherwise \end{cases} \quad (9)$$

In the following numerical simulation, the frequency f=150 kHz and the number of cycles N=5 were used. An aluminum plate (E=73 GPa, ν=0.33, ρ=2700 kg/m^3, h=1.0 mm) is used with sensor radius a= 2.5 mm. A 2 mm diameter circular hole is located at (x_d, y_d)=(450 mm, 450 mm). The wave propagation and time reversal operation is carried out between Sensor A and B. The use of f=150 kHz will generate both A0 and S0 Lamb waves. The single A0 mode, however, can be generated in real situation, for instance, by using two sensors attached on both sides of plate or by using a variable angle beam transducer. Another method for generating a single mode Lamb wave is to use PZT sensors with mode tuning by adjusting the frequency. Considering this situation, only the A0 mode for generation and propagation was used in the simulation.

The response signal received at sensor B is shown in Fig. 4(c). The received signal is composed of the direct wave and the scattered wave. Even the narrowband input signal causes a velocity dispersion on the A0 mode propagation at a propagation distance of 300 mm. When the response signal is reversed in time and reemitted to the input sensor, the velocity dispersion of Lamb wave is compensated as shown in Fig. 4(d). Two side bands appear with respect to the main signal. It is noted from eqn. (4) that $\bar{t}_{12}$ and $\bar{t}_{21}$ are the same time shift with the opposite signs $\bar{t}_{12}$ = -$\bar{t}_{21}$, and this is clearly reflected on a symmetric pair of the side bands in Fig. 5. The time difference $\bar{t}_{mn}$ between the main mode and one of the side band is calculated as $(r_2-r_1)/\overline{V}_g = (d_A+d_B-d_{AB})/\overline{V}_g = (0.3\sqrt{2}-0.3)$

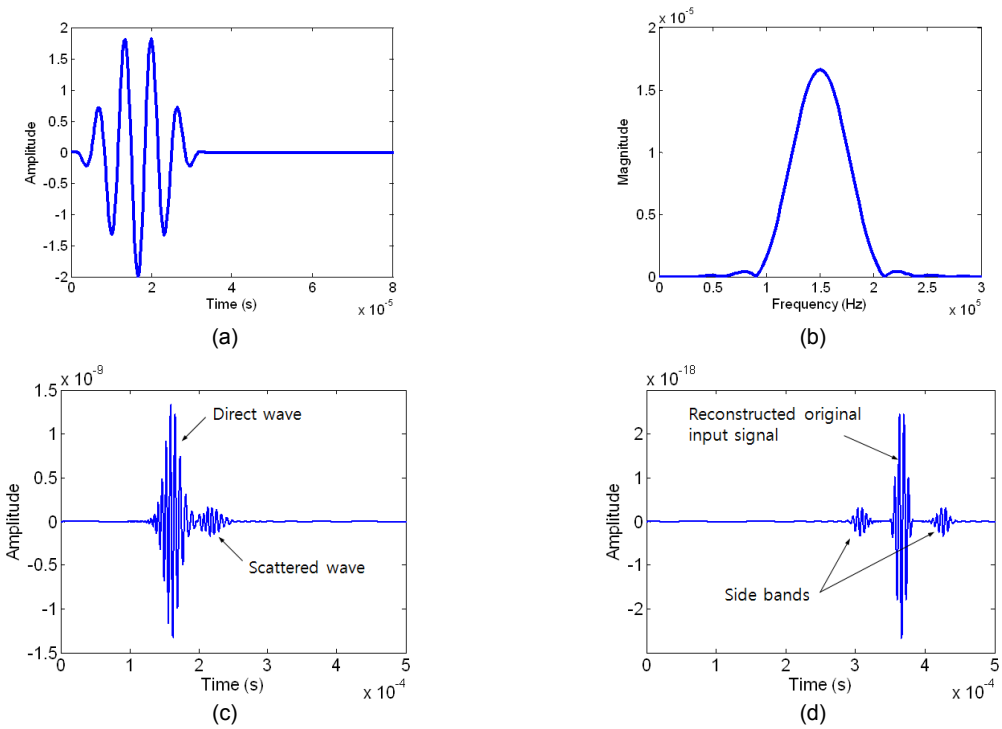

Fig. 4 Time reversal process of a narrowband toneburst waveform. (a) Time domain input signal (b) Its magnitude spectrum, (c) Response signal of sensor B at the propagation distance r=300 mm, and (d) Reconstructed TR signal compared with the original input signal

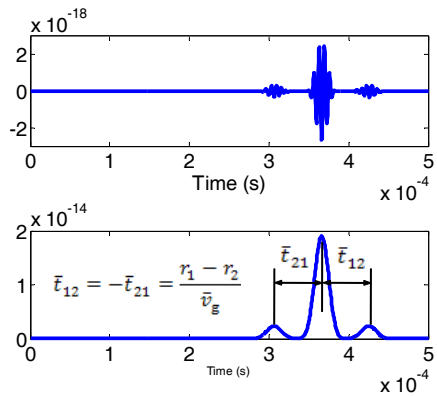

Fig. 5 Arrival time difference between the main mode signal and the side bands after time reversal reconstruction of the received output signal at sensor B

/2069=60 μs. From Fig. 5, this time difference is also estimated to be 60 μs from the time-frequency analysis. The reconstructed input signal is magnified in the vicinity of the main mode and compared to the original input signal in Fig. 6. For the better comparison of the signal's shape, the reconstructed and original input signals in Fig. 6 are normalized so that their maximum values are equal to 2.0. The shape of the reconstructed main mode is practically identical to that of the original input signal.

Fig. 7 shows the time-frequency spectrum of the reconstructed defect signal (one of the side band signal) after time reversal of the output

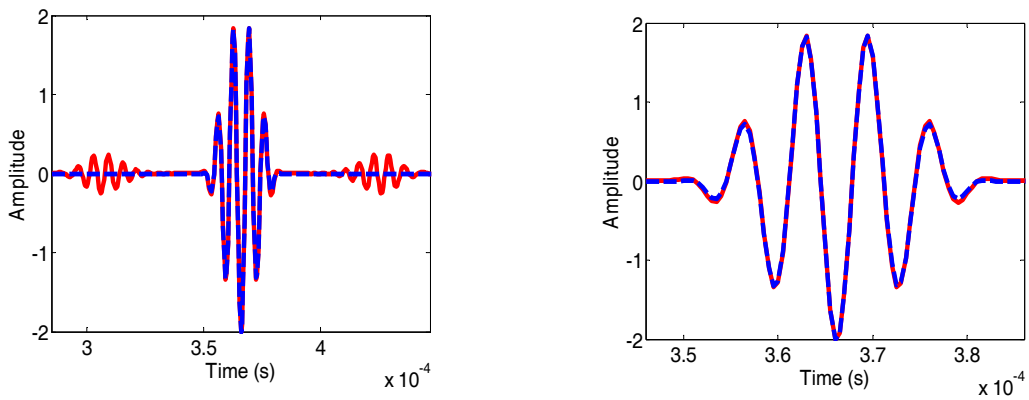

Fig. 6 The shape of the reconstructed main mode completely recovers the original input signal

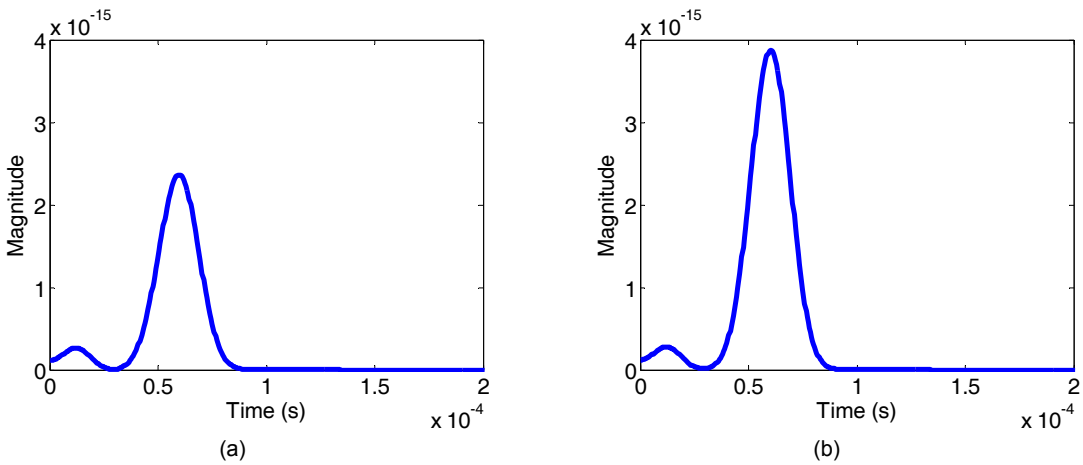

Fig. 7 Reconstructed defect signal: (a) For sensor pair A and B; (b) For sensor pair A and C

signal and subtraction of the original input signal for sensor pair A-B and A-C, respectively. They correspond to defect scattering for 90 and 0 degrees in Fig 1, respectively, and well reflects the scattering amplitude difference at these angles. These spectra will be used for reconstructing the defect localization image.

The reconstructed defect localization image is shown in Fig. 8(a), where the circular through hole of 1 mm radius is located at the center of the sensor network, (x_d, y_d)=(450 mm, 450 mm). It shows that the reconstructed defect localization

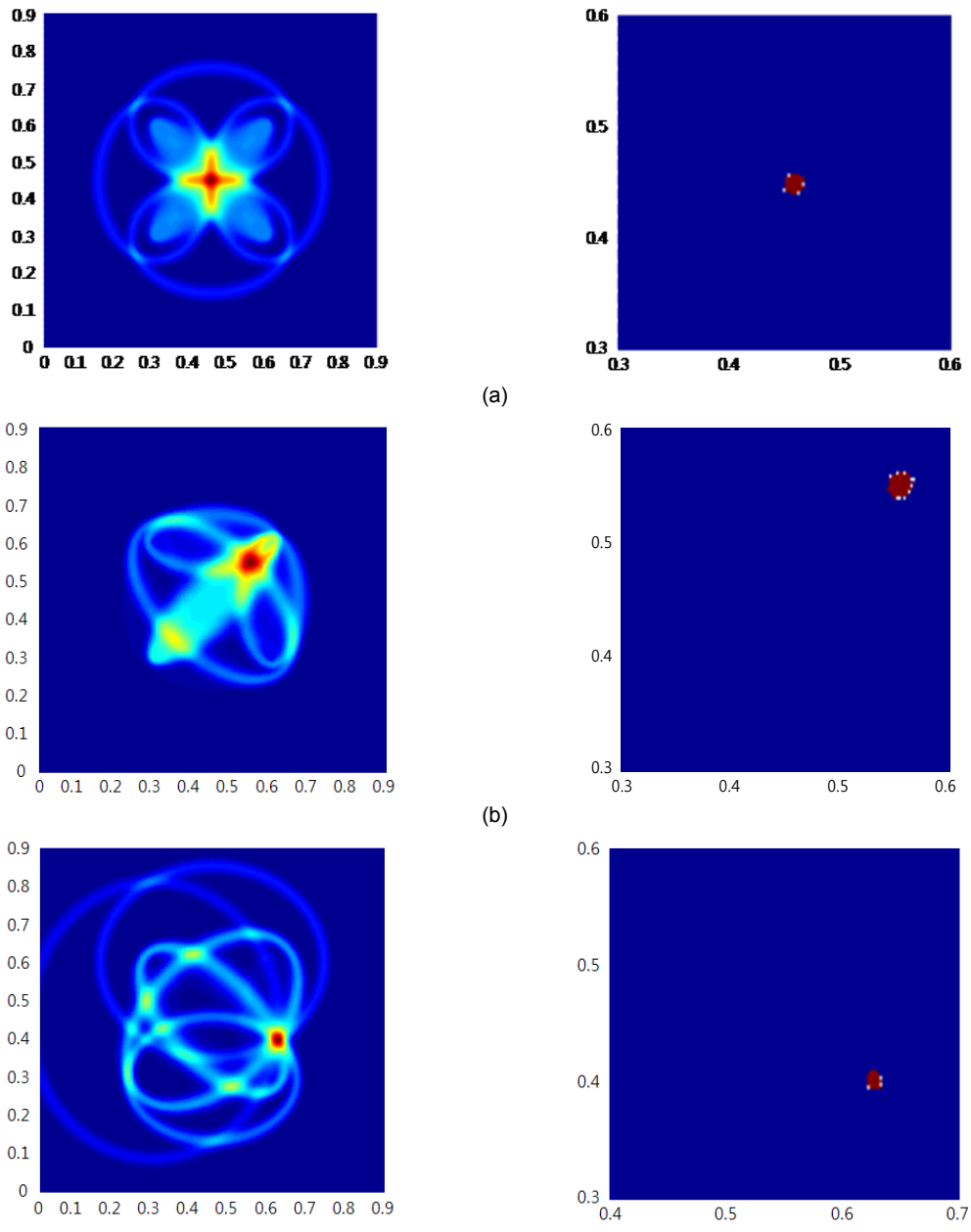

Fig. 8 Defect localization image and its binary image: (a) Circular through hole of radius r =1 mm radius and defect location= (450 mm, 450 mm), (b) Circular through hole of radius r = 1 mm radius and defect location = (550 mm, 550 mm), and (c) Circular through hole of radius r = 2 mm radius and defect location = (620 mm, 400 mm)

image accurately locates the defect. This defect reconstruction is obtained by superimposing the images of different actuator/sensor signal paths. Fig. 8 shows a binary image created by only accounting for image pixels whose intensity is larger than an arbitrary threshold value, which in this study was chosen as 90% of the maximum intensity of the reconstructed defect localization image.

The next case aims to study the performance of Lamb wave-based defect detection methodology under a situation where the defect is located relatively close to one of the transducers in order to verify the robustness of the proposed methodology. Fig. 8(b) shows the reconstructed defect localization image and corresponding binary image when the circular hole of 1 mm radius is located at (x_d, y_d)=(550 mm, 550 mm).

The last numerical simulation deals with a case when the defect is located outside of the transducer network, i.e., (x_d, y_d)=(620 mm, 400 mm). The reconstructed defect localization image and corresponding binary image are shown in Fig. 8(c). This case again highlights the robustness of detecting and locating defect using the proposed Lamb wave-based defect detection methodology.

If reflections from boundaries of the plate are included, they will generate additional side bands in the reconstructed waveform. They are not considered in this work to avoid the complexity of the problem. These side bands will also form defect-like images. Since the positions of boundaries are known, these images can be differentiated from the actual defect image. If sensors are placed close to the boundary, and if times-of-flight to the defect and to the boundary are about the same, then the defect image cannot be easily separated from the images of boundaries. The reflection problem is beyond the scope of current work, and will be addressed in other work.

6. Conclusions

A baseline-free imaging for detection and location of a defect in plates were studied in this work. The proposed method employed the time reversal of flexural waves and a beam-forming technique using a distributed network of transducers operating in a pitch-catch mode. The time reversal of the output signal which contains the direct and scattered waves recovered the original input signal and produced additional side bands. One of the side band was used to form the baseline-free defect localization image. Based on the fundamental idea of the beamforming method with a distributed sensors, the signal-to-noise ratio of the defect image was greatly improved. Several defect localization images were simulated, and the results showed excellent agreements with actual defect locations. Experimental studies will be needed to verify the proposed method and to be applied to real structures.

References

Alleyne, D. N., Pavlakovic, B., Lowe, M. J. S. and Cawley, P. (2001), Rapid, Long-Range Inspection of Chemical Plant Pipework Using Guided Waves, *Review of Progress in QNDE*, Vol. 20, pp. 180-187

Cuc, A., Gougiutiu, V., Joshi, S. and Tidwell, Z. (2007), Structural Health Monitoring with Piezoelectric Wafer Active Sensors for Space Applications, *AIAA Journal*, Vol. 45, pp. 2838-2850

Giurgiutiu, V., Zagrai, A. and Bao, J. (2004), Damage Identification in Aging Aircraft Structures with Piezoelectric Wafer Active Sensors, *Journal of Intelligent Material Systems and Structures*, Vol. 15, pp. 673-687

Giurgiutiu, V. (2008) *Structural Health Monitoring with Piezoelectric Wafer Active Sensors*, Academic Press, New York

Jeong, H. (2010) A Lamb Wave Time Reversal Technique for Defect Localization Imaging in Plate-Like Structures, Submitted to Smart Materials and Structures

Ihn, J. B. and Chang, F. K. (2008) Pitch-Catch Active Sensing Methods in Structural Health Monitoring for Aircraft Structures, *Structural Health Monitoring*, Vol. 7, pp. 5-15

Ing, R. and Fink, M. (1998) Time-Reversed Lamb Waves, *IEEE transactions on Ultrasonics, Ferro-electrics, and Frequency Control*, Vol. 45, pp. 1032-1043

Norris, A. N. and Vemula, C. (1995), Scattering of Flexural Waves on Thin Plates, *Journal of Sound and Vibration*, Vol. 181, pp. 115-125

Park, S., Yun, C. B., Roh, Y. and Lee, J. J. (2006), PZT-Based Active Damage Detection Techniques for Steel Bridge Components, *Smart Materials and Structures*, Vol. 13, pp. 873-879

Park, H. W., Kim, S. B. and Sohn, H. (2009), Understanding a Time Reversal Process in Lamb Wave Propagation, *Wave Motion*, Vol. 46, pp. 451-467

Prasad, S. M., Balasubramaniam, K. and Krishnamurthy, C. (2004), Structural Health Monitoring of Composite Structures Using Lamb Wave Tomography, *Smart Materials and Structures*, Vol. 13, pp. 873-879

Rose, J. L., Ditri, J. J., Pilarski, A., Rajana, K. and Carr, F.T. (1994), Guided Wave Inspection Technique for Nuclear Steam Generator Tuning, *NDT&E International*, Vol. 27, pp. 307-310

Tua, P., Quek, S. and Wang, Q. (2005), Detection of Cracks in Cylindrical Pipes and Plates Using Piezo-Actuated Lamb Waves, *Smart Materials and Structures*, Vol. 14, pp. 1325-1342

Wang, C. H., Rose, J. T. and Chang, F. K. (2004), Synthetic Time-Reversal Imaging Method for Structural Health Monitoring, *Smart Materials and Structures*, Vol. 13, pp. 415-423

Santani, G. B., Yu, L., Xu, B. and Giurgiutiu, V. (2007), Lamb Wave-Mode Tuning of Piezo-Electric Wafer Active Sensors for Structural Health Monitoring, *Journal of Vibration and Acoustics*, Vol. 129, pp. 752-762

Sohn, H., Park, G., Wait, J. R., Limback, N. P. and Farrar, C. R. (2004). Wavelet-Based Active Sensing for Delamination Detection in Composite Structures, *Smart Materials and Structures*, Vol. 13, pp. 153-160

Sohn, H., Park, H. W., Law, K. H. and Farrar, C. R. (2007), Damage Detection in Composite Plates by Using an Enhanced Time Reversal Method, *Journal of Aerospace Engineering*, Vol. 20, pp. 141-151